Journal of Casting & Materials Engineering Vol. 2 No. 1 (2018) 14–23
http://dx.doi.org/10.7494/jcme.2018.2.1.14

Comparison among Different Constitutive Equations on Investigating Tensile Plastic Behavior and Microstructure in Austempered Ductile Iron

Giuliano Angella[a]*, Franco Zanardi[b]

[a] National Research Council of Italy (CNR), Institute of Condensed Matter Chemistry and Technologies for Energy (ICMATE), Via R. Cozzi 53, 20125 Milan (MI), Italy
[b] Zanardi Fonderie S.p.A., Via Nazionale 3, 37046 Minerbe (VR), Italy
e-mail: giuliano.angella@cnr.it

Received: 12 January 2018/Accepted: 21 February 2018/Published online: 30 March 2018

Abstract

The capabilities of different constitutive equations of approximating the tensile flow curves and correlating plastic behavior with the microstructure were investigated in austempered ductile iron ADI 1050. In a previous paper, the microstructure evolution of ADI 1050 during austempering was investigated through quenching the ADI 1050 after 14 increasing austempering times to room temperature. The 14 samples were tensile tested and two classes of constitutive equations were examined in the present paper. The Hollomon-type constitutive equations approximated all of the tensile flow curves of ADI 1050 very well but failed in correlating the plastic behavior with microstructure evolution. Voce-type constitutive equations approximated the tensile flow curves only at high stresses very well but could correlate the plastic behavior with the microstructure evolution of ADI 1050 during austempering excellently. The reason of this success was rationalized in terms of the physical basis of Voce-type equations, while Hollomon-type equations are empirical.

Keywords:

tensile testing, mechanical properties, constitutive equations, microstructure, austempered ductile irons

1. INTRODUCTION

Solid state transformations are involved in most material industrial production, where a material's microstructure is designed to provide the desired properties. The minimal mechanical properties concerning the plastic behavior of metallic materials are yield strength (YS), ultimate tensile strength (UTS), and elongation to rupture (A5) [1, 2]. However, an analysis of the tensile plastic behavior through appropriate constitutive equations could give more-precise information on the material's microstructure. In fact, flow stress and the strain hardening rate (that is, flow stress increase with straining) are sensitive to a material's microstructure, so a plastic behavior analysis can be used to follow solid state transformations like austempering in ductile irons (DIs) [3–15].

Austempered ductile irons (ADIs) are ductile irons produced through proper alloying and heat-treatments, and they present excellent mechanical properties due to an ausferritic microstructure consisting of BCC α ferrite Widmanstätten acicular laths and metastable FCC γ with a high content of C (commonly indicated as γ_{HC}) [11]. The austempering process consists of austenitization at high temperature (800–920°C) followed by quenching and holding the material in a salt bath at lower temperatures (250–400°C) for austempering transformation $\gamma \rightarrow \alpha + \gamma_{HC}$ [8, 13], with a final quenching to room temperature. However, for longer austempering times, the high-carbon austenite decomposes into ferrite α and carbide Fe-C ε' [10, 11], causing the embrittlement of ADI. So, optimal ausferrite is produced after proper austempering times that define a time interval called the *process window* [14, 15].

Several constitutive equations have been proposed to describe the tensile flow curves at room temperature of metallic materials. These equations can be classified into two main categories: a) Hollomon-type equations, which are power law relationships between true flow stress σ and true plastic strain ε_p (Hollomon [16], Swift [17], Ludwik [18], and Ludwigson [19]); and b) Voce-type equations, which are exponential decay relationships between σ and ε_p (Voce [20], Sah [21]). Though all of these constitutive equations have been proposed as empirical equations, Hollomon-type equations have no specific physical bases, whilst Voce-type parameters can be related to microstructural features, since a wide body of research results have given physical meaning to the differential forms of Voce-type equations [22–27] (which are also known as dislocation-density-related constitutive equations) [26].

The present paper aims to compare the results from using different constitutive equations in analyzing the tensile plastic behavior of an ADI 1050 quenched to room temperature after 14 different austempering times.

The microstructure evolution of ADI 1050 was deeply investigated through optical microscopy (OM), the electron backscattered diffraction (EBSD) technique, and transmission electron microscopy (TEM); these results have been reported elsewhere [15]. When ADI 1050 was quenched before the austempering transformation ended, a significant fraction of hard and brittle martensite was also found in ausferrite, while carbides Fe-C ε' were found after quenching to room temperature after too-long austempering times [15]. The tensile plastic behavior of ADI 1050 is expected to reflect the different microstructures obtained after quenching at different austempering times. The comparison concerned two aspects: a) the capability of the constitutive equations to approximate the tensile flow curves; and b) the capability of correlating the constitutive equation parameters to the different microstructures in order to describe the austempering evolution of ADI 1050 reported in [15].

2. MATERIAL AND RESEARCH METHODOLOGY

ADI 1050 [2] with a nodular graphite volume fraction of 10 ± 1 % was first austenitized then quenched and held in a salt bath at the austempering temperature and finally quenched to room temperature after 14 different increasing times (t_1, t_2, ..., t_{14}). The austempering times were selected in order to stop the austempering transformation before its end, to have proper ausferrite after the end of austempering, and to have carbides Fe-C ε′ after longer austempering times. The actual values of the austempering times are not indicated and arbitrary units are reported, as the aim of the investigation concerns the capabilities of different constitutive equations to approximate the tensile flow curves from ADI 1050 with different microstructures and correlate the constitutive equation parameters with the microstructure. Detailed results concerning the microstructure evolution results are reported in [15]. The ADI 1050 microstructure after the proper austempering time is reported in Figure 1a. It comes into nodular graphite (black) with ausferrite consisting of α (bright) and γ_{HC} (dark) lamellae.

Tensile tests were carried out complying to ASTM E8-8M at room temperature and strain rate 10^{-4} s^{-1} on samples with initial gauge diameter d_o = 12.5 mm and gauge length l_o = 50 mm. True stress σ vs. true strain ε were considered, which are $\sigma = S\cdot(1 + e)$ and $\varepsilon = \ln(1 + e)$, with S and e the engineering stress and strain, respectively. For strain hardening analysis, only the plastic component of strain was considered through subtracting elastic strain $\varepsilon_e = \sigma/E$ (E is the experimental Young modulus) to overall strain ε, which is $\varepsilon_p = \varepsilon - \varepsilon_e$. Constitutive equations were fitted to the true plastic flow curves before the Considére's criterion, which is $d\sigma/d\varepsilon_p = \sigma$ if it occurred, as beyond this condition, the flow curves were not representative of the material's behavior. In Figure 1b, selected tensile flow curves σ vs. ε_p of the 14 ADI 1050 samples are reported.

The shapes of the flow curves changed significantly during the austempering transformation. During the early stages of austempering, that is, the austempering time interval (t_1–t_4), when austempering was not ended and the volume fractions of martensite obtained with quenching to room temperature decreased [15], the tensile flow curves had specific shapes with pronounced concavity. Beyond t_4, the elastic-plastic transition was sharper and the flow curves increased slowly, showing a little concavity. Apparently, no significant change of plastic behavior took place between t_6 and t_{14}, even if carbides Fe-C ε' were observed at t_{14} [15]. Indeed, YS, UTS, and elongations to rupture vs. austempering time also did not show any trend that could relate the mechanical properties to the ADI 1050 microstructure's evolution during austempering [15].

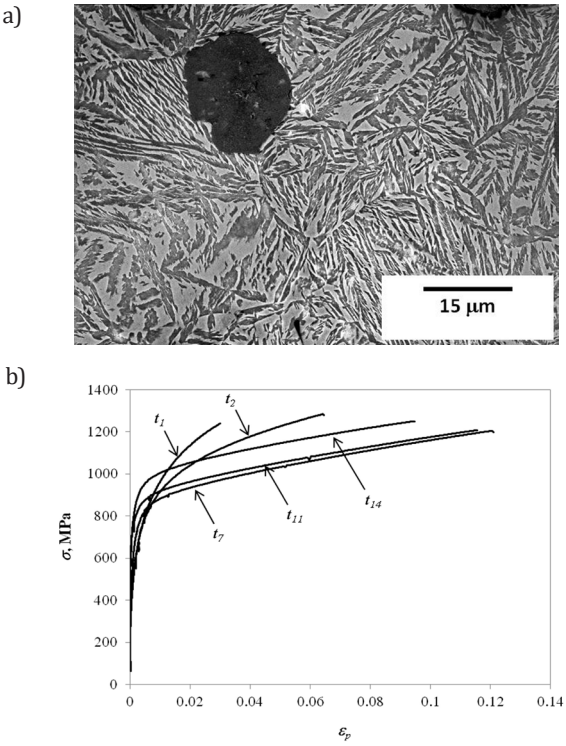

Fig. 1. ADI 1050: a) proper ausferritic microstructure with graphite nodule (black), α (bright) and γ_{HC} (dark); b) selected tensile flow curves of samples after different austempering times

3. THEORETICAL BACKGROUND: CONSTITUTIVE EQUATIONS

3.1. Hollomon equation [16]

The Hollomon equation is defined as:

$$\sigma = K_H \cdot \varepsilon_p^{\,n} \tag{1}$$

where:

K_H – strength coefficient, MPa;
n – strain hardening exponent.

Hollomon parameters K_H and n are found through plotting the experimental $\sigma - \varepsilon_p$ data in a Log-Log plot.

Since a proper linear region is generally not found in the Log(σ) – Log(ε_p) data, the strain range on which the Hollomon equation has to be fitted is arbitrary. In the present work, the Hollomon equation was fitted to the tensile flow curves beyond strain $\varepsilon_{p,in} = 0.002$ until the strain to rupture or the strain of Considére's criterion.

3.2. Ludwigson equation [19]

Among all the other Hollomon-type constitutive equations, the Ludwigson one is considered here because of the successful use in describing DI's flow curves [10, 28, 29]. The equation is defined as:

$$\sigma = K_H \cdot \varepsilon_p^{\,n} \pm K_o \cdot \exp\left(K_L + n_L \cdot \varepsilon_p\right) \tag{2}$$

where:

K_H – strength coefficient, MPa;
n – strain hardening exponent;
K_o – 1 MPa (for dimensional consistency);
K_L – dimensionless parameter;
n_L – dimensionless parameter.

The exponential part (conventionally indicated as Δ) has been introduced to improve the usual significant bad fitting at small strains of the Hollomon part with the experimental σ – ε_p data.

3.3. Voce equation [20]

The Voce equation is defined as:

$$\sigma = \sigma_v + \left(\sigma_0 - \sigma_v\right) \cdot \exp\left(-\frac{\varepsilon_p}{\varepsilon_c}\right) \tag{3}$$

where:

σ_V – saturation stress, MPa;
ε_c – characteristic transient strain;
σ_o – back-extrapolated stress at $\varepsilon_p = 0$, MPa.

σ_V is achieved asymptotically with straining, ε_c defines the rate with which σ_V is approached, and σ_o is the stress at $\varepsilon_p = 0$. σ_V can be defined as the theoretical strength achievable if no geometrical instabilities occurred during mechanical testing (that is, necking in tensile testing). The differential form of Equation (3) is:

$$\frac{d\sigma}{d\varepsilon_p} = \frac{\sigma_v}{\varepsilon_c} - \frac{\sigma}{\varepsilon_c} = \Theta_v - \frac{\sigma}{\varepsilon_c} \tag{4}$$

where:

Θ_V – back-extrapolated strain hardening rate at σ = 0, MPa.

According to Equation (4), there is a linear relationship between ($d\sigma/d\varepsilon_p$) and σ, since Θ_V and ($1/\varepsilon_c$) are constant during straining [22–24]; so, a linear region in the plot ($d\sigma/d\varepsilon_p$) vs. σ of the experimental data has to be found to work out parameters Θ_V and ($1/\varepsilon_c$) (which usually occurs at high stresses). Finally, σ_o is determined by fitting Equation (3) to the experimental tensile flow curves, with ($1/\varepsilon_c$) and σ_V found from the strain hardening analysis.

3.4. Kocks–Mecking–Estrin (KME) equation

When the material has a high density of precipitation and interfaces obstructing the dislocation motion [24, 26], the following equation should be used:

$$\sigma = \sigma_E^{\,2} + \left(\sigma_0^{\,2} - \sigma_E^{\,2}\right) \cdot \exp\left(-\frac{\varepsilon_p}{\varepsilon_c}\right)^{\frac{1}{2}} \tag{5}$$

where:

σ_E – saturation stress, MPa;
ε_c – characteristic transient strain;
σ_o – back-extrapolated stress at $\varepsilon_p = 0$ MPa.

Though this equation was first proposed by Sah [21] for describing high temperature flow curves, Kocks–Mecking and Estrin [22–27] later gave the basis for its physical interpretation; here onwards, Equation (5) is called the KME equation. Analogously to the Voce equation, σ_E is the saturation stress that is achieved asymptotically with straining, ε_c is the characteristic transient strain that defines the rate with which σ_E is approached, and σ_o is the back-extrapolated stress at $\varepsilon_p = 0$. Also in this case, σ_E can be defined as the theoretical strength achievable if no geometrical instabilities occurred during mechanical testing. In order to find the characteristic equation parameters, the plot ($2\sigma \cdot d\sigma/d\varepsilon_p$) vs. σ^2 has to be analyzed [24, 26]. In fact, the differential form of Equation (5) is:

$$2\sigma\frac{d\sigma}{d\varepsilon_p} = \frac{\sigma_E^{\,2}}{\varepsilon_c} + \frac{\sigma^2}{\varepsilon_c} = \Theta_E - \frac{\sigma^2}{\varepsilon_c} \tag{6}$$

where:

Θ_E – back-extrapolated squared strain hardening rate at σ = 0 MPa

According to Equation (6), there is a linear relationship between ($2\sigma \cdot d\sigma/d\varepsilon_p$) and σ^2, since σ_E and ($1/\varepsilon_c$) are constant during straining. Therefore, the σ – ε_p range to fit the Estrin equation is not arbitrary, but a linear region in the experimental data ($2\sigma \cdot d\sigma/d\varepsilon_p$) vs. σ^2 has to be found (which usually occurs at high stresses). Finally, σ_o is worked out by fitting Equation (5) to the experimental tensile flow curves, with ($1/\varepsilon_c$) and σ_E found from the strain hardening analysis.

4. RESULTS

4.1. Hollomon-type constitutive equations: fitting results

The fitting procedures of the Hollomon and Ludwigson equations with the resulting curves that best approximated in the experimental tensile flow curves of ADI 1050 after the selected austempering times are reported in Figures 2–4. Initial strain $\varepsilon_{p,in}$ for the Hollomon parameter determination was set to 0.002 for all flow curves. The best Hollomon fit for the experimental tensile flow curve at austempering time t_7 is reported in Figure 2, for example. The fits did not approximate the experimental flow curves perfectly. Similar results were found for tensile flow curves from the other austempering times regardless of the presence of martensite at short austempering times or carbides Fe-C ε' at t_{14} [15].

Two examples of Ludwigson equation fits are reported in Figures 3 and 4 for austempering times t_1 and t_7, respectively.

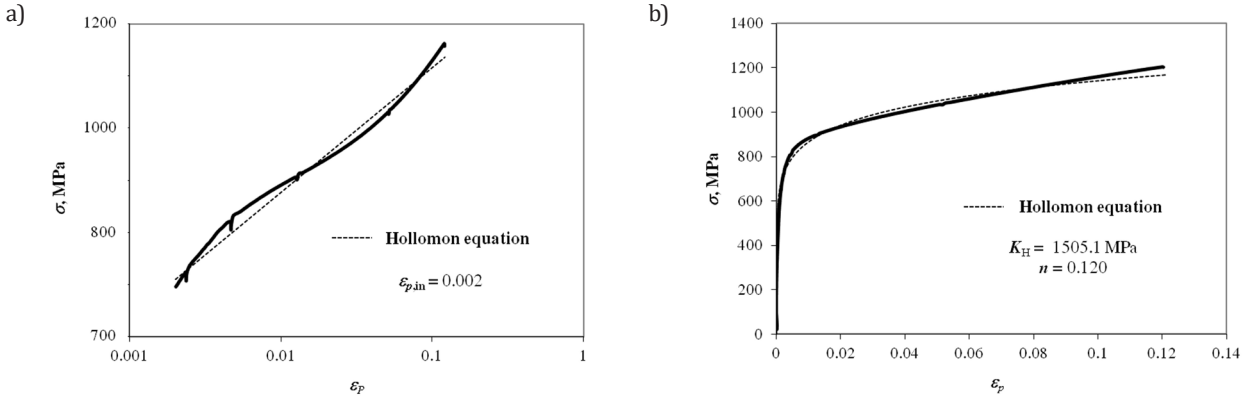

Fig. 2. Tensile flow curve data of ADI 1050 at austempering time t_7: a) Log(σ) vs. Log(ε_p) with Hollomon best linear fit with $\varepsilon_{p,in}$ = 0.002; b) experimental tensile flow curve with best approximating Hollomon equation

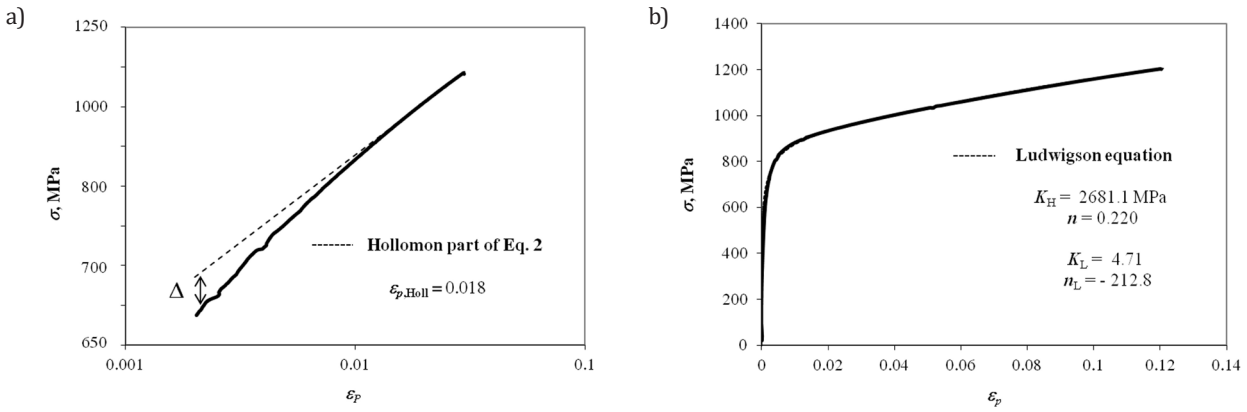

Fig. 3. Tensile flow curve data of ADI 1050 at austempering time t_1: a) Log(σ) vs. Log(ε_p) with Ludwigson best linear fit with $\varepsilon_{p,Holl}$ = 0.018 for Hollomon part determination, while Δ is exponential component of Ludwigson equation Eq. (2); b) experimental tensile flow curve with best approximating Ludwigson equation

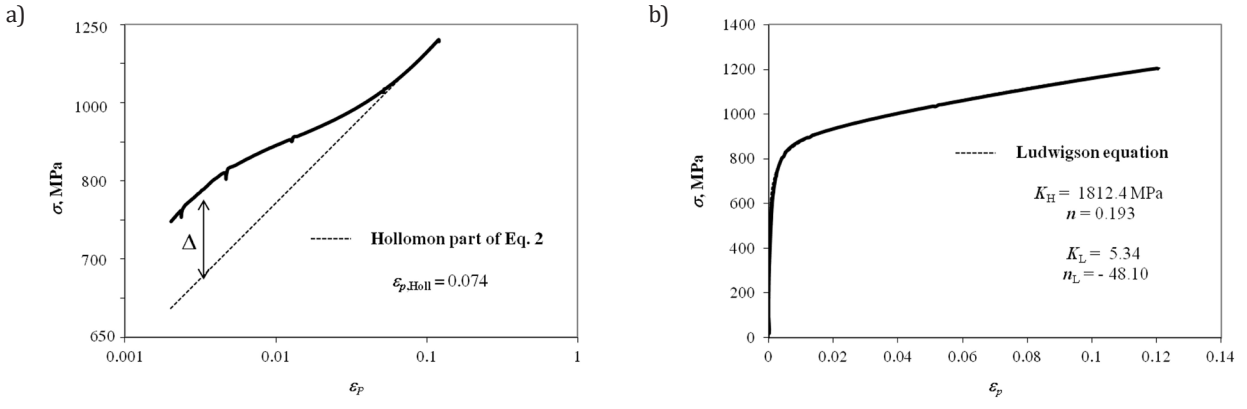

Fig. 4. Tensile flow curve data of ADI 1050 at austempering time t_7: a) Log(σ) vs. Log(ε_p) with Ludwigson best linear fit with $\varepsilon_{p,Holl}$ = 0.074 for Hollomon part determination; b) experimental tensile flow curve with the best approximating Ludwigson equation

In this case, there is no ambiguity in the choice of the strain ranges for the Hollomon parts of Equation (4). In fact, beyond $\varepsilon_{p,Holl} = 0.018$ for t_1 and 0.074 for t_7 until rupture, there was linearity in the plot Log(σ) vs. Log(ε_p). Exponential part Δ was negative for the t_1 flow curve and positive for t_7. Compared to the Hollomon equation, Ludwigson equations appeared to excellently approximate the experimental flow curves from yielding to rupture. Similar results are for the tensile flow curves from the other austempering temperatures regardless the presence of martensite at short austempering times or carbides Fe-C ε' at t_{14} [15].

4.2. Voce-type constitutive equations: fitting results

The procedures for determining the best Voce and KME equations of the tensile flow curve of ADI 1050 after selected austempering time t_7 are reported in Figures 5 and 6, respectively. In the Voce procedure, the best linear fit was applied to the linear region of the differential data ($d\sigma/d\varepsilon_p$) vs. σ at high stresses in Figure 5a, while for the KME equation, the best linear fit was applied to the linear region of the differential data ($2\sigma \cdot d\sigma/d\varepsilon_p$) vs. σ^2 at high stresses in Figure 6a. Though the best fits were excellent at high stresses, both the Voce and KME equations failed at low stresses (and small strains).

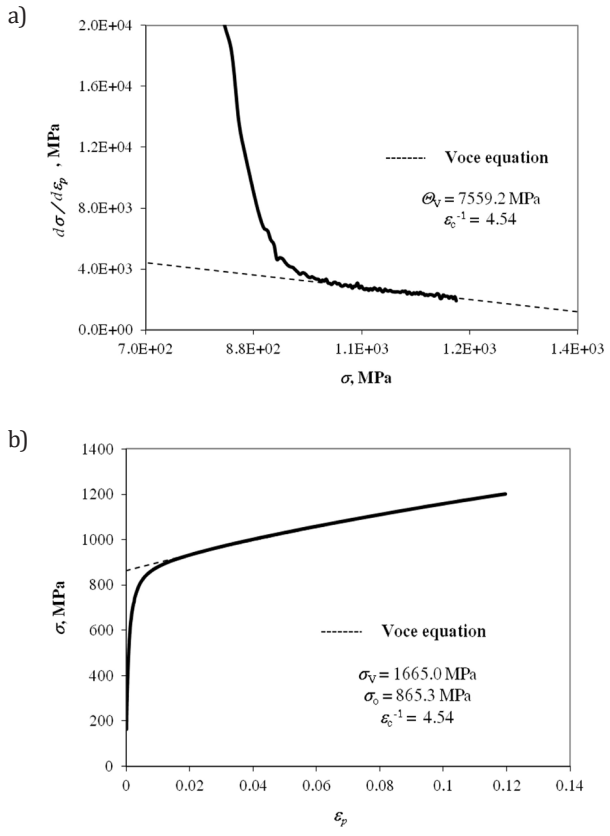

Fig. 5. Tensile flow curve data of ADI 1050 at austempering time t_7: a) ($d\sigma/d\varepsilon_p$) vs. σ with differential Voce best linear fit at high stresses; b) experimental tensile flow curve with best approximating Voce equation

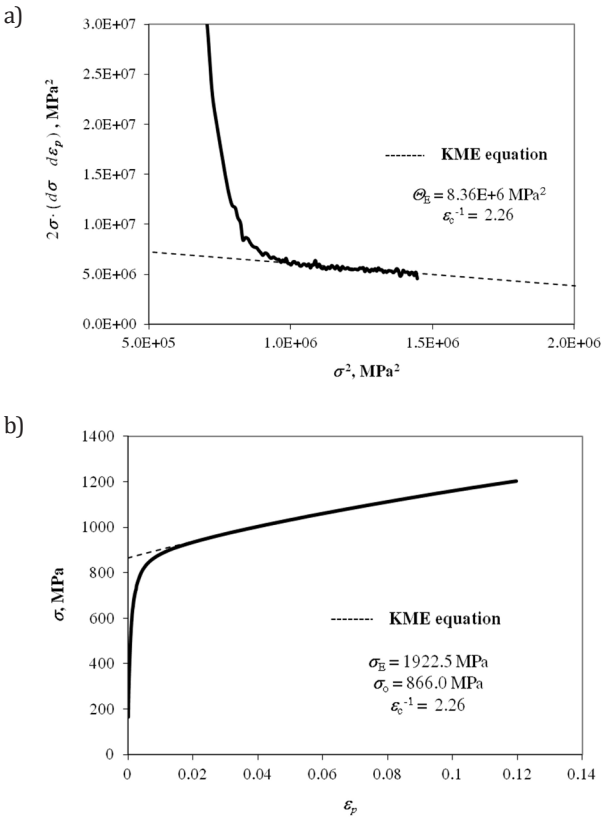

Fig. 6. ADI 1050 at austempering time t_7: a) ($2\sigma \cdot d\sigma/d\varepsilon_p$) vs. σ^2 with differential KME best linear fit at high stresses; b) experimental tensile flow curve with best approximating Estrin equation

4.3. Hollomon-type constitutive equations: correlation between constitutive equation parameters and microstructure evolution

The parameters of the Hollomon-type constitutive equations were found for all of the tensile flow curves from the 14 samples of ADI 1050 quenched from austempering to room temperature. Then, the parameters were plotted against the austempering time in Figures 7–10. In Figure 7, Hollomon parameters K_H and n decreased continuously from the beginning of austempering until the end of the transformation. The K_H and n trends seemed to indicate that, after the early stages of the transformation, , that is, the austempering time interval (t_1–t_4), when significant volume fractions of martensite were produced through quenching [15], the plastic behavior of ADI 1050 was independent on longer austempering times, showing no particular trend that could indicate the achievement of optimal ausferrite at intermediate austempering times or the precipitation of carbides Fe-C ε' at t_{14} [15].

The characteristic parameters of the Ludwigson equation are reported in Figure 8. K_H and n showed a clear decrease with austempering time, that is, the austempering time interval (t_1–t_4), while K_L and n_L did not show any particular trend. Though the significant reduction of K_H and n at shorter austempering times was consistent with the martensite volume fraction reduction, no change of the Ludwigson parameters related to carbide Fe-C ε' precipitation at longer times could be detected.

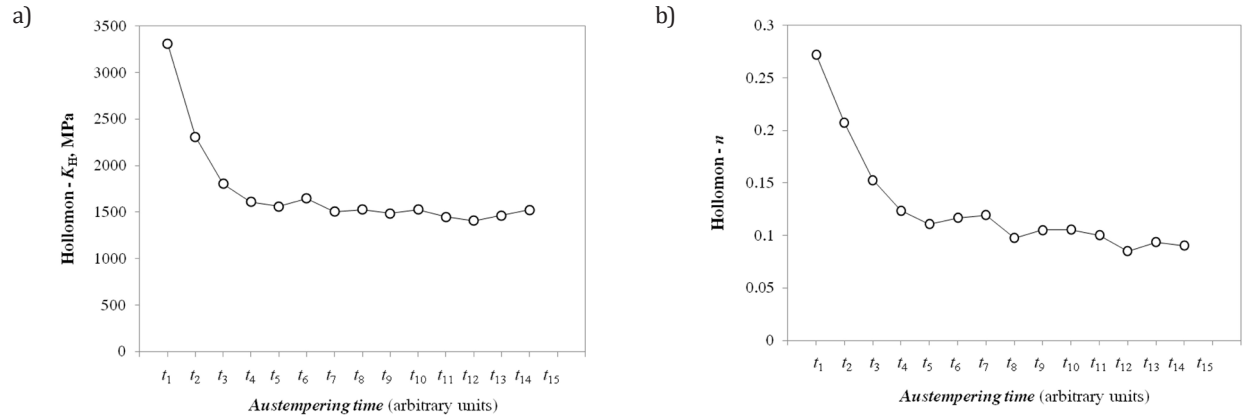

Fig. 7. Characteristic parameters of Hollomon equation: a) strength coefficient K_H vs. austempering time; b) strain hardening exponent n vs. austempering time

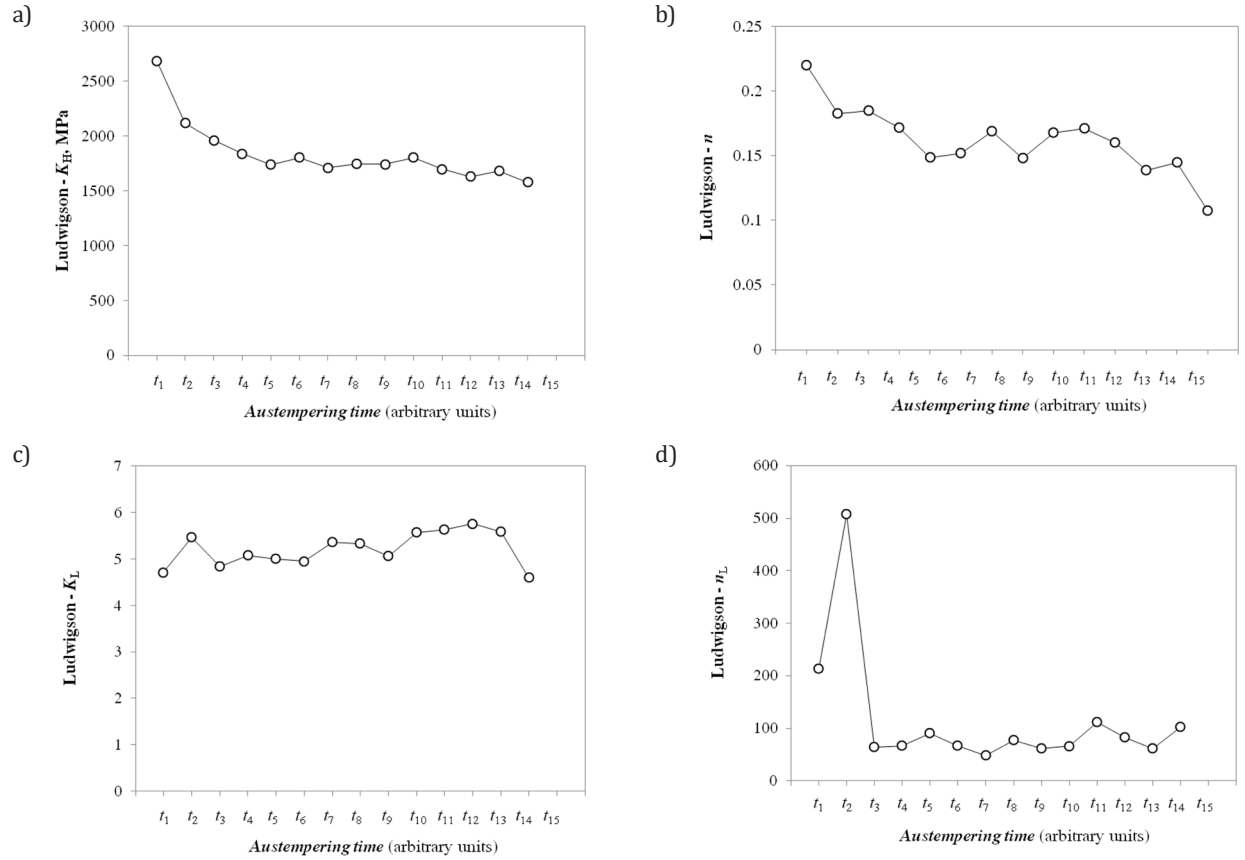

Fig. 8. Characteristic parameters of Ludwigson equation: a) K_H vs. austempering time; b) n vs. austempering time; c) K_L vs. austempering time; d) n_L vs. austempering time

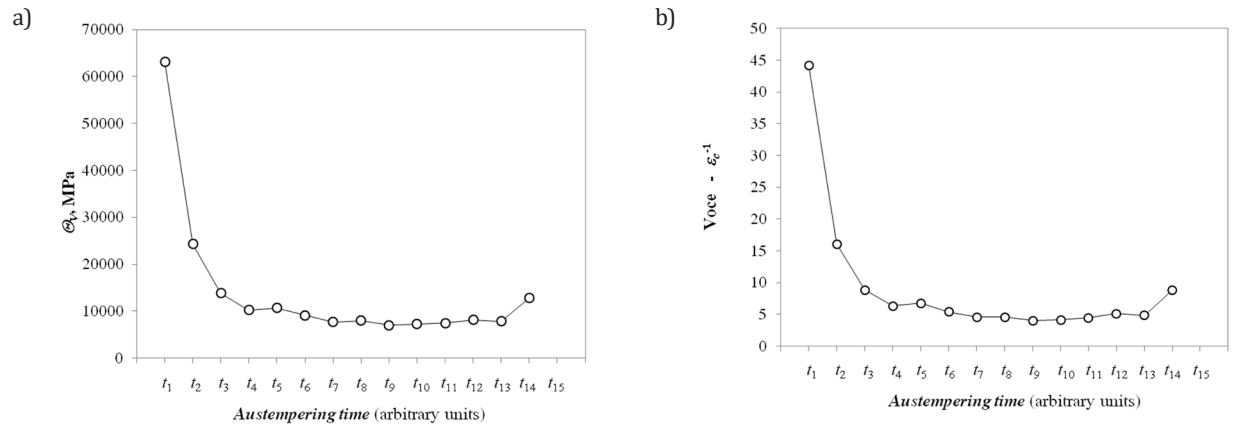

Fig. 9. Characteristic parameters of Voce equation: a) Θ_V vs. austempering time; b) $(1/\varepsilon_c)$ vs. austempering time

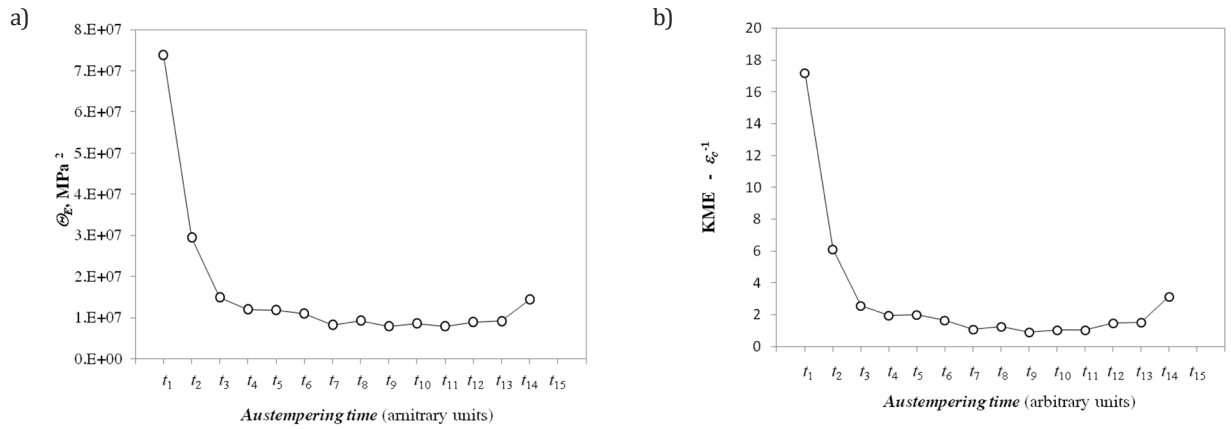

Fig. 10. Characteristic parameters of KME equation: a) Θ_E vs. austempering time; b) $(1/\varepsilon_c)$ vs. austempering time

4.4. Voce-type constitutive equations: correlation between constitutive equation parameters and microstructure evolution

Voce parameters Θ_V and $(1/\varepsilon_c)$ in Equation (4) and KME parameters Θ_E and $(1/\varepsilon_c)$ in Equation (6) are reported in Figures 9 and 10, respectively. In Figure 9, the Voce parameters seemed to be consistent with the microstructure evolution of ADI 1050 during austempering. Θ_V and $(1/\varepsilon_c)$ decreased initially according to the martensite volume fraction reduction and increased slightly with longer austempering times, showing minima approximately at the same austempering time (t_9). The change of the plastic behavior at longer austempering time was consistent with the carbide Fe-C ε' precipitation observed through TEM at t_{14} [15].

Also, KME parameters Θ_E and $(1/\varepsilon_c)$ decreased initially according to the martensite volume fraction reduction and increased slightly with longer austempering times, showing minima approximately at the same austempering time (t_9), consistent with the Voce equation. Therefore, the KME parameters also seemed to be consistent with the microstructure evolution of ADI 1050 during the austempering reported in [15].

5. DISCUSSION

5.1. Capability of constitutive equations in approximating tensile flow curves

A comparison among the different constitutive equations on the capabilities of approximating the tensile flow curves of ADI 1050 with different microstructures was reported in Paragraph 4.1. The Hollomon fitting procedure was straightforward, even if the arbitrariness on determining the experimental strain range on which the Hollomon equation could be fitted was a drawback (since the Hollomon parameters depend on $\varepsilon_{p,in}$). However, the Hollomon equation provided good approximations of the whole tensile flow curves of ADI 1050. The Ludwigson fitting procedure was more-complex; however, there was no arbitrariness in the experimental strain range on which the Hollomon parts of Equation (2) were fitted. Indeed, the Ludwigson equation excellently approximated all of the tensile flow curves of ADI 1050 with different microstructures from yielding to rupture. These results agree with the evidence already reported in the literature on DIs [10, 28, 29].

The fitting procedures of the Voce-type equations were more-complex since the differential data had to be considered and the linear regions had to be found for fitting the differential forms of the Voce and KME equations. However, at low stresses, considerable parts of the experimental differential data were not well-described by Equations (4) and (6), while the fits at high stresses were excellent. As a consequence, the experimental tensile flow curves in Figures 5b and 6b were well-fitted with the Voce-type equations only at high strains. This discrepancy at low stresses has also been reported in ductile materials like copper [23] and stainless steel [30] and has been attributed to a transient of the dislocation structure evolution with straining [23, 30]. In DIs the interpretation of this discrepancy could be more-complex, since soon after yielding the decohesion of the interface between the graphite nodules and the matrix occurs. This decohesion gives rise to the nucleation of voids that then grow, and finally coalesce, which should significantly affect the DIs tensile flow curve. However, despite the large damage because of the void coalescence, no dramatic drop of tensile stress occurs in DIs [31, 32]. Indeed, a detailed strain hardening investigation has proven that the tensile flow curves of DIs at high stresses are representative of the microstructure of DIs [33], so Voce-type equations could be fitted to the experimental flow curves at high stresses (high strains). However, further investigations should be needed to rationalize the contribution of the void nucleation to the flow curves at yielding.

However, despite the fact that the Ludwigson equation described excellently the whole tensile flow curves, there is indeed a fundamental problem with the application of the Hollomon-type equations. The fitting procedures to find the equation parameters are based on Log(σ) vs. Log(ε_p); that is, on plastic strain ε_p that is an ill-defined parameter [22, 34] since it depends on the thermo-mechanical history of the material (heat treatments and pre-strain).

For instance, if the sample ADI 1050 at t_7 was hypothetically reloaded during tensile testing after 0.060 and 0.075, two other flow curves that are distinct from the monotonic flow curve can be found (as reported in Figure 11).

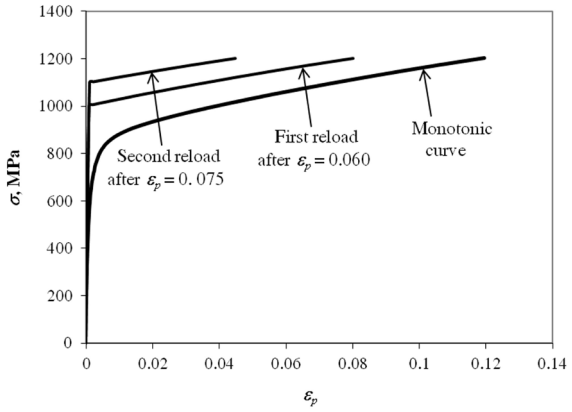

Fig. 11. ADI 1050 at austempering time t_7: monotonic curve and hypothetical reloaded flow curves after 0.060 and 0.075 pre-strains

The Ludwigson and Voce equations could be fitted on the reloaded flow curves to work out the equation parameters. In Table 1, the results of K_H and n for the Ludwigson equation and σ_V and $(1/\varepsilon_c)$ for the Voce equation are reported together with the results from the monotonic curve for comparison. The Ludwigson parameters change significantly with increasing pre-strain, and the percentage variations achieve –17.2% for K_H and –62.7% for n after the pre-stain 0.075 with respect to the monotonic equation parameters. This proves that the Ludwigson parameters are not material constants since they depend on the pre-strains (the mechanical history). This is true for all Hollomon-type equations since their fitting procedures are based on strain. On the contrary, the application of Voce-type equations is based on the analysis of the experimental differential data ($d\sigma/d\varepsilon_p$) vs. σ, which have been reported to be in good approximation independent on the thermo-mechanical history of materials [22, 34]. Consistently, Voce parameters Θ_V and $(1/\varepsilon_c)$ of each reloaded tensile flow curve are similar in the range of the experimental error of the differential analyses, being the percentage variations with respect to monotonic equation parameters –5.6% for Θ_o and –8.1% for $(1/\varepsilon_c)$ after the pre-stain 0.075. So, Voce parameters Θ_V and $(1/\varepsilon_c)$ (and Θ_E and $(1/\varepsilon_c)$ for the KME equation for which the fitting procedure is also based on differential data analysis) are material constants independent of the pre-strains.

5.2. Capability of constitutive equations in correlating equation parameters and microstructure

A comparison among the constitutive equations on their capabilities of correlating the plastic behavior with the microstructure evolution of ADI 1050 during austempering was reported in Paragraph 4.2. The Hollomon-type equation parameters in Figures 7 and 8 could describe the ADI 1050 microstructure evolution reported in [15]. Though general decreasing trends of the Hollomon-type parameters at short austempering times, that is, the austempering time interval (t_1–t_4), seemed to be consistent with the martensite volume fraction reduction, the trends did not catch the carbide Fe-C ε' precipitation at t_{14} [15]. The reason for the failure in the correlating plastic behavior with the microstructure evolution has to be attributed to the empirical nature of Hollomon-type constitutive equations. Indeed, attempts have been made to provide a physical interpretation of the Ludwigson equation [19]. The Hollomon part of Equation (2) was related to the proper dislocation cell structure built up during deformation, while the exponential part at low stresses (small strains) was related to the planar slip with no dislocation structure typical of low stacking fault materials like stainless steel [35, 36]. However, as reported in Figures 3 and 4, exponential deviation Δ of Equation (2) can be positive or negative, confirming the lack of real physical bases. However, as proven above, the determination of the parameters through using fitting procedures where the plastic strain is considered is the most-significant confirmation of a lack of physical bases of the Hollomon-type equations.

Table 1
Ludwigson and Voce equation parameters found through fitting flow curves of ADI 1050 at austempering time t_7 in Figure 11 after two different reloadings: first, after ε_p = 0.60, and second, after ε_p = 0.75. Percentage variation Δ (%) of parameters are calculated with respect to monotonic parameters

Curve	Ludwigson parameters				Voce parameters			
	K_H, MPa	ΔK_H, %	n	Δn, %	Θ_o, MPa	$\Delta\Theta_o$, %	$1/\varepsilon_c$	$\Delta(1/\varepsilon_c)$, %
Monotonic	1812.4	–	0.193	–	7559.2	–	4.54	–
First reload	1659.5	–8.4	0.127	–34.2	7008.2	–7.3	4.06	–10.6
Second reload	1501.5	–17.2	0.072	–62.7	7133.2	–5.6	4.17	–8.1

Conversely, Voce-type constitutive equation parameters could describe the ADI 1050 microstructure evolution during austempering. Even if the Voce equation was first proposed as an empirical equation in 1948 [20], the mechanistic interpretation of strain hardening proposed by Kocks–Mecking [22–24] and Estrin [25–27] (see [14, 15, 37] for DIs) has given physical meaning to the differential forms of Voce and KME equations (Eqs. (4) and (6), respectively). The characteristic parameters of these equations can be correlated to the dislocation theory and microstructure of materials, and they are in fact well-known as dislocation-density-related constitutive equations [26] (among which, the Voce equation is the best-known). On these physical bases, parameters Θ_V and Θ_E are athermal components of strain hardening because of dislocation multiplication and storage and are inversely proportional to the mean free path of mobile dislocations that, in turn, are correlated to microstructural features like dislocation cells, average grain size, and average spacing λ between the geometric obstacles and precipitates. Based on the KME equation, a detailed calculation of λ with austempering time in the present ADI 1050 is reported in [15]. The found values of λ were numerically consistent with the ADI 1050 microstructure. The dynamic recovery terms $(1/\varepsilon_c)$ depend strongly on the dislocation properties and, in turn, on the crystallographic lattice where the mobile dislocations move. The crystallographic structure, chemical composition, and stacking fault energy are the parameters that mainly affect the dislocation cores and, as a consequence, the dynamic recovery rate [24, 38]. So, Voce-type constitutive equations have robust physical bases, which explains their capability of correlating plastic behavior with the microstructure evolution in ADI 1050 during austempering.

6. CONCLUSIONS

A comparison among different constitutive equations on their capabilities of approximating the tensile flow curves of ADI 1050 with different microstructures as well as the correlating plastic behavior and ADI 1050 microstructure evolution during austempering have been reported. The following conclusions can be stated:

- though the Hollomon equation could fit the tensile flow curves of ADI 1050 with different microstructures from yielding to rupture quite well, the Ludwigson equation fits of the experimental tensile flow curves were excellent;
- Voce-type equations perfectly fit the tensile flow curves at high stresses (high strains) while failing at low stresses (small strains) soon after yielding;
- though Hollomon-type equations better fit the tensile flow curves, it should be kept in mind that Hollomon-type equation parameters are not material constants but depend significantly on the mechanical history (an example of the pre-strain effects on the equation parameters was given);
- Voce-type equations could excellently correlate plastic behavior with the microstructure evolution of ADI 1050 during austempering, while the Hollomon-type equations failed;
- the reason for this success is due to the physical bases of the differential forms of Voce-type equations.

In conclusion: if the aim is to approximate all of the tensile flow curves of ADI 1050, the Ludwigson constitutive equation should be used, even if the limits related to the empirical nature of the equation should always be remembered. For microstructure investigations, Voce-type equations have to be used because of their robust physical bases and can be useful tools in validating the solid state transformations involved in material industrial production.

Acknowledgements

Mr. E. Veneri, F. Vettore, and S. Masaggia from R&D Laboratory Zanardi Fonderie S.p.A. as well as Mr. Ranucci and Della Torre from ICMATE-CNR are warmly thanked for their technical support.

REFERENCES

[1] ISO 1083:2004(E), *Spheroidal graphite cast irons – Classification*.
[2] ISO 17804:2005(E), *Founding – Ausferritic spheroidal graphite cast irons – Classification*.
[3] Kim Y.J., Shin H., Park H. & Lim J. (2008). Investigation into mechanical properties of austempered ductile cast iron (ADI) in accordance with austempering temperature. *Materials Letters*, 62, 357–360.
[4] Hernández-Rivera J.L., Campos Cambranis R.E. & De la Garza A. (2011). Study of microstructural evolution and mechanical properties exhibited by non alloyed ductile iron during conventional and stepped austempering heat treatment. *Materials & Design*, 32, 4756–4762.
[5] Basso A., Sikora J. & Martinez R. (2013). Analysis of mechanical properties and its associated fracture surfaces in dual-phase austempered ductile iron. *Fatigue & Fracture of Engineering Materials and Structures*, 36, 650–659.
[6] Blackmore P.A. & Harding R.A. (1984). The effects of metallurgical process variables on the properties of austempered ductile irons. *Journal of Heat Treating*, 3/4, 310–325.
[7] Fernandino D.O., Massone J.M. & Boeri R.E. (2013). Characterization of the austemperability of partially austenitized ductile iron. *Journal of Materials Processing Technology*, 213, 1801–1809.
[8] Yang J. & Putatunda S.K. (2004). Influence of a novel two-step austempering process on the strain-hardening behavior of austempered ductile cast iron (ADI). *Materials Science & Engineering A*, 382, 265–279.
[9] Basso A., Martínez R. & Sikora J. (2011). Influence of chemical composition and holding time on austenite (γ) Ferrite (α) transformation in ductile iron occurring within the intercritical interval. *Journal of Alloys and Compounds*, 509, 9884–9889.
[10] Olofsson J., Larsson D. & Svensson I.L. (2011). Effect of Austempering on Plastic Behavior of Some Austempered Ductile Iron Alloys. *Metallurgical and Materials Transactions A*, 42, 3999–4007.
[11] Meena A. & El Mansori M. (2012). Material Characterization of Austempered Ductile Iron (ADI) Produced by a Sustainable Continuous Casting-Heat Treatment Process. *Metallurgical and Materials Transactions A*, 43, 4755–4766.

[12] Smallman R.E., Harris I.R. & Duggan M.A. (1997). Microstructure and materials processing. *Journal of Materials Processing Technology*, 63, 18–29.
[13] Fredriksson H., Stjerndahl J. & Tinoco J. (2005). On the solidification of nodular cast iron and its relation to the expansion and contraction. *Materials Science & Engineering A*, 413, 363–372.
[14] Angella G., Donnini R., Bonollo F., Fabrizi A. & Zanardi F. (2017). Assessment of austempering process evolution through tensile testing. *La Metallurgia Italiana*, 6, 11–17.
[15] Donnini R., Fabrizi A., Bonollo F., Zanardi F. & Angella G. (2017). Assessment of the microstructure evolution of an austempered ductile iron during austempering process through strain hardening analysis. *Metals and Materials International*, 23, 855–864.
[16] Hollomon J.H. (1945). Tensile Deformation. *Transactions of the Metallurgical Society of AIME*, 162, 268–290.
[17] Swift H.W. (1952). Plastic Instability under Plane Stress. *Journal of the Mechanics and Physics* of *Solids*, 1, 1–18.
[18] Ludwik P. (1909). *Elemente der Technologischen Mechanik*. Leipzig: Verlag Von Julius, Springer.
[19] Ludwigson D.C. (1971). Modified stress-strain relation for FCC metals and alloys. *Metallurgical Transactions*, 2, 2825–2828.
[20] Voce E. (1948). The relationship between stress and strain in homogenous deformation. *Journal of the Institute of Metals*, 74, 537–562.
[21] Sah J.P., Richardson G.J. & Sellars C.M. (1969). Recrystallisation during hot deformation of Ni. *Journal of Australian Institute of Metals*, 14, 292–297.
[22] Kocks U.F. (1976). Laws for work-hardening and low-temperature creep. *Journal of Engineering Materials and Technology*, 98, 76–85.
[23] Kocks U.F. & Mecking H. (1981). Kinetics of flow and strain-hardening. *Acta Metallica*, 29, 1865–1875.
[24] Kocks U.F. & Mecking H. (2003). Physics and phenomenology of strain hardening: the FCC case. *Progress in Materials Science*, 48, 171–273.
[25] Estrin Y. & Mecking H. (1984). A unified phenomenological description of the work hardening and creep based on one-parameter models. *Acta Metallica*, 32, 57–70.
[26] Estrin Y. (1996). Dislocation density related constitutive modelling. In: Krausz A.S. and Krausz K. (Eds.): *Unified constitutive laws of plastic deformation*. Elsevier, 69–106.
[27] Estrin Y. (1998). Dislocation theory based constitutive modelling: foundations and applications. *Journal of Materials Processing Technology*, 80–81, 33–39.
[28] Selin M. (2010). Comparing Three Equations Used for Modeling the Tensile Flow Behavior of Compacted Graphite Cast Irons at Elevated Temperatures. *Metallurgical and Materials Transactions A*, 41, 2805–2815.
[29] Svensson I.L. & Salomonsson K. (2017). *11th International Symposium on Science and Processing of Cast Iron – SPCI-XI*, 4–7 September 2017, Jönköping, Sweden. Proceedings in press.
[30] Angella G., Donnini R., Maldini M. & Ripamonti D. (2014). Combination between Voce formalism and improved Kocks–Mecking approach to model small strains of flow curves at high temperatures. *Materials Science & Engineering A*, 594, 381–388.
[31] Dong M.J., Prioul C. & Francois D. (1997). Damage effect on the fracture toughness of nodular cast iron: part I. Damage characterization and plastic flow stress modelling. *Metallurgical and Materials Transactions A*, 28, 2245–2254.
[32] Guillemer-Neel C., Feaugas X. & Clavel M. (2000). Mechanical behavior and damage kinetics in nodular cast iron: part I. Damage mechanisms. *Metallurgical and Materials Transactions A*, 31, 3063–3074.
[33] Guillemer-Neel C., Feaugas X. & Clavel M. (2000). Mechanical behavior and damage kinetics in nodular cast iron: part II. Hardening and damage. *Metallurgical and Materials Transactions A*, 31, 3075–3086.
[34] Reed-Hill R.E., Crebb W.R. & Monteiro S.N. (1973). Concerning the analysis of tensile stress-strain data using Log($d\sigma/d\varepsilon_p$) versus Log(σ) diagram. *Metallurgical and Materials Transactions A*, 4, 2665–2667.
[35] Choudhary B.K., Samuel E.I., Rao K.B.S. & Mannan S.L. (2001). Tensile stress-strain and work hardening behaviour of 316LN austenitic stainless steel. *Materials Science and Technology*, 17, 223–231.
[36] Samuel K.G. & Rodriguez P. (2005). On power-law type relationships and the Ludwigson explanation for the stress-strain behaviour of AISI 316 stainless steel. *Journal of Materials Science*, 40, 5727–5731.
[37] Angella G., Zanardi F. & Donnini R. (2016). On the significance to use dislocation-density-related constitutive equations to correlate strain hardening with microstructure of metallic alloys: the case of conventional and austempered ductile irons. *Journal of Alloys and Compounds*, 669, 262–271.
[38] Hull D. & Bacon D.J. (2002). *Introduction to dislocations*, Publisher Butterworth-Heinemann.